[PS]Porosity Evolution in the Bassein Limestone of Panna and Mukta Fields, Offshore Western India: Burial Corrosion and Microporosity Development*

Andrew J. Barnett[1], V. Paul Wright[2,3] and Mohit Khanna[4]

Search and Discovery Article #50326 (2010)
Posted September 30, 2010

*Adapted from poster presentation at AAPG Annual Convention and Exhibition, New Orleans, Louisiana, April 11-14, 2010

[1]BG Group, Thames Valley Park, RG6 1PT, U.K (andrew.barnett@bg-group.com)
[2]BG Group, Thames Valley Park, RG6 1PT, U.K
[3]Department of Earth Sciences, Cardiff University, Park Place, Cardiff, CF10 3YE, U.K
[4]BG India, BG House, Lake Boulevard, Hiranandi Business Park, Puwai, Mumbai, India

Abstract

The Bassein Formation Eocene-Oligocene ramp carbonates are examples of formerly tight limestones in which all current porosity was produced at depth by burial corrosion. In the Panna Field dissolution created extensive breccia pipes and collapse features hundreds of metres in diameter. These appear to be associated with NNW-SSE trending strike-slip faults. Similar large-scale structures have not been identified in Mukta Field. However, both Panna and Mukta underwent a phase of selective corrosion, dissolving stylolites, stylolite-associated fractures and preferentially removing micrite matrix and finely crystalline grains such as miliolids and agglutinated foraminifera to produce extensive microporosity. This microporosity differs from the micro-rhombic calcite mosaics documented by some authors in Middle Eastern Cretaceous microporous carbonate reservoirs in that individual crystals show clear signs of dissolution (e.g. rounding) and enlarged pore throat diameters. This difference is also reflected in poroperm trends which are distinct from those of microporous Shuaiba reservoirs in Oman and the U.A.E. The causal late stage corrosion post-dated saddle dolomite growth and was followed by locally extensive dickite precipitation. This suite of diagenetic features and the paragenetic sequence are consistent with a mixing corrosion model of porosity development. Mass balance considerations and the TOC of the Panna-Mukta source rock preclude the possibility of major dissolution by acidic fluids generated from CO_2 or carboxylic acids.

The data presented here point to a spectrum of microporosity development from: (1) chalk reservoirs in which intra- and interparticle microporosity is hosted in pelagic nanno- and microfossils, (2) matrix and intraparticle microporosity occurring in relatively pristine (i.e. mainly non-leached) micro-rhombic calcite mosaics and (3) corrosion-enhanced matrix and intraparticle microporosity in which individual calcite crystals have been rounded and reduced in size giving a concomitant increase in pore throat diameter relative to non-leached micro-rhombic calcite mosaics.

Porosity Evolution in the Bassein Limestone of Panna and Mukta Field, Offshore Western India: Burial Corrosion and Microporosity Development

Andrew J. Barnett[1], V. Paul Wright[1 & 2] & Mohit Khanna[3]

1. BG Group, Thames Valley Park, RG6 1PT, U.K.
2. Department of Earth Sciences, Cardiff University, Park Place, Cardiff, CF10 3YE, U.K.
3. BG India, BG House, Lake Boulevard, Hiranandi Business Park, Puwai, Mumbai, India

1. Abstract

The Bassein Formation Eocene-Oligocene ramp carbonates are examples of formerly tight limestones in which all current porosity was produced at depth by burial corrosion. In the Panna Field dissolution created extensive breccia pipes and collapse features hundreds of metres in diameter. These appear to be associated with NNW-SSE trending strike-slip faults. Similar large-scale structures have not been identified in Mukta Field. However, both Panna and Mukta underwent a phase of selective corrosion, dissolving stylolites, stylolite-associated fractures and preferentially removing micrite matrix and finely crystalline grains such as miliolids and agglutinated foraminifera to produce extensive microporosity. This microporosity differs from the micro-rhombic calcite mosaics documented by some authors in Middle Eastern Cretaceous microporous carbonate reservoirs in that individual crystals show clear signs of dissolution (e.g. rounding) and enlarged pore throat diameters. This difference is also reflected in poroperm trends which are distinct from those of microporous Shuaiba reservoirs in Oman and the U.A.E. The causal late stage corrosion post-dated saddle dolomite growth and was followed by locally extensive dickite precipitation. This suite of diagenetic features and the paragenetic sequence are consistent with a mixing corrosion model of porosity development. Mass balance considerations and the TOC of the Panna-Mukta source rock preclude the possibility of major dissolution by acidic fluids generated from CO_2 or carboxylic acids.

The data presented here point to a spectrum of microporosity development from: (1) chalk reservoirs in which intra- and interparticle microporosity is hosted in pelagic nanno- and microfossils, (2) matrix and intraparticle microporosity occurring in relatively pristine (i.e. mainly non-leached) micro-rhombic calcite mosaics and (3) corrosion-enhanced matrix and intraparticle microporosity in which individual calcite crystals have been rounded and reduced in size giving a concomitant increase in pore throat diameter relative to non-leached micro-rhombic calcite mosaics.

2. Introduction

The Panna and Mukta Fields are located in the Bombay Basin in central west offshore India (Fig. 1). Panna Field is located *ca*. 50 km east of the giant Bombay High Field and 95 km west of Bombay. It lies immediately north of the giant Bassein gas field, separated by a shallow syncline. Water depth ranges from 45 to 55 m. Panna Field is a broad, low relief anticlinal trap (Fig. 2). The oil column is *ca*. 20 m thick and largely in transition to water. It is sandwiched between a gas cap and a 40 to 60 m thick water leg. The gas column is typically 50 m thick.

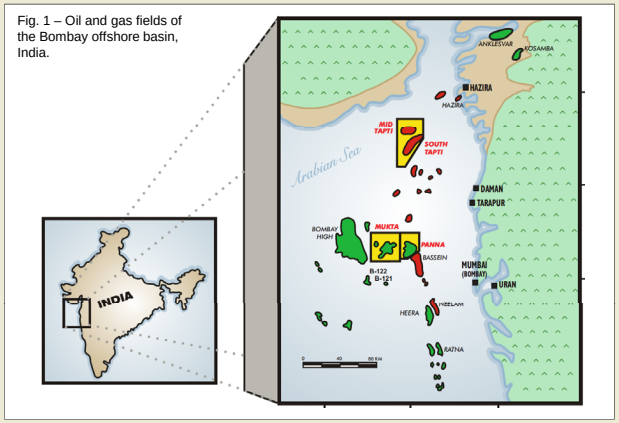

Fig. 1 – Oil and gas fields of the Bombay offshore basin, India.

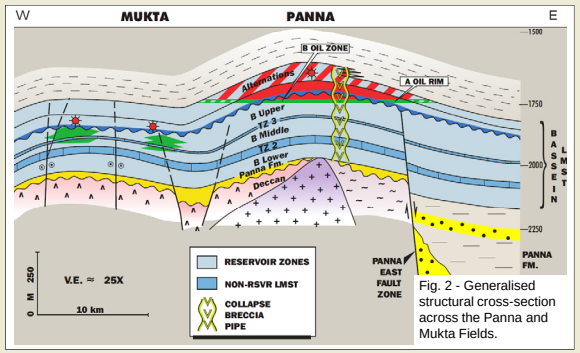

Fig. 2 - Generalised structural cross-section across the Panna and Mukta Fields.

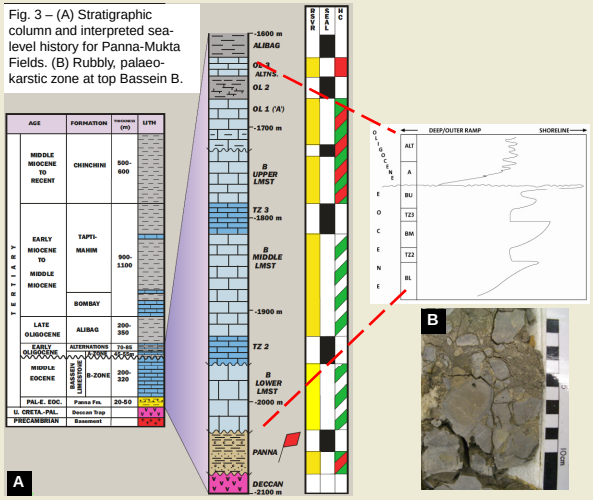

Fig. 3 – (A) Stratigraphic column and interpreted sea-level history for Panna-Mukta Fields. (B) Rubbly, palaeo-karstic zone at top Bassein B.

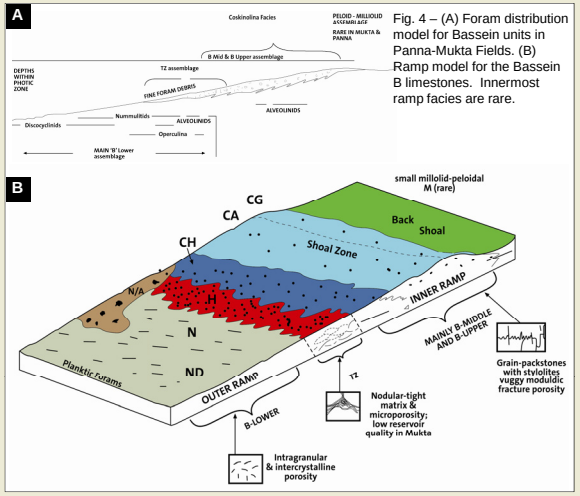

Fig. 4 – (A) Foram distribution model for Bassein units in Panna-Mukta Fields. (B) Ramp model for the Bassein B limestones. Innermost ramp facies are rare.

The Mukta Field is located 15 km west of Panna Field. Water depth is *ca*. 65 m. Production is from three stacked oil pools within several anticlinal closures.

The principal hydrocarbon-bearing formations in both the Panna and Mukta fields are the Eocene Bassein B and Early Oligocene Bassein A limestones. However, porosity development is less continuous in the Mukta area. The Bassein reservoirs are sourced by the Paleocene-Early Eocene deltaic clastics of the Panna Formation. The seal comprises the Late Oligocene Alibag Shale.

3. Geological Setting

Sedimentation in the Bombay Basin occurred in a passive margin setting of Late Cretaceous to recent age. The Tapti-Surat Depression (northeast) and the adjacent Mahim Graben (east) comprise the Late Tertiary clastic depocentre as well as the probable source areas for hydrocarbons. The Mahim Graben is separated from the Panna Field by the Panna East fault zone. This is the major structural feature in the Panna-Mukta blocks. It was an extensional fault through Late Eocene time and has undergone a episode of transpression during the post-Mid Miocene.

The deposition of the Eocene-Early Oligocene limestones of Panna-Mukta took place on an unusual platform configuration of what appears to be an isolated (detached), southerly dipping ramp. This is supported by the absence of a shelf margin or resedimentation as sediment gravity flows. However, shoreline facies appear to be absent.

Approximately 95 % of these limestones are dominated by foraminifera. Sedimentary structures are very infrequent. Consequently, the facies scheme is largely based on the presence, abundance and preservation state of foraminifera. Fig. 4 illustrates the likely relationship of these foraminifera distributions. The bulk of the limestones in the Bassein B are composed of the *Coskinolina* assemblage and identifying clear depth trends is difficult. The component subfacies cover a range of depths from above fair-weather wave base in inner ramp settings to probable mid-ramp depths. The complex inter-fingering of the different *Coskinolina* subfacies suggests that the facies pattern was more of a mosaic than one with shore-parallel facies belts. Despite the presence of an uncomformity associated with minor palaeokarstic features capping the Bassein B interval, this appears to have had little impact on reservoir quality.

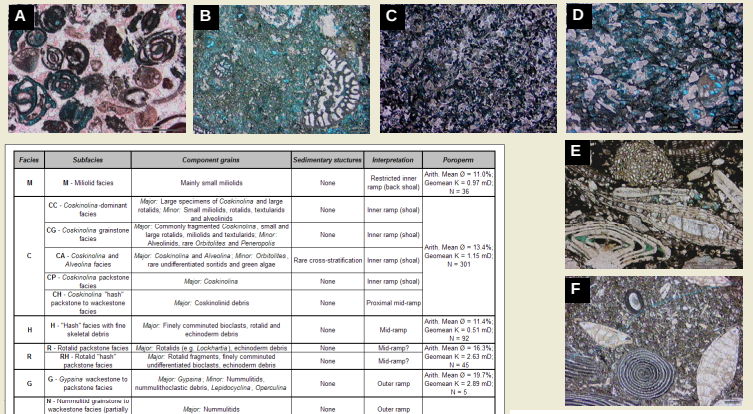

Fig. 5 – Representative photo-micrographs of principal facies types (*cf.* Table 1 for details). (A) Facies M. (B) Facies C. (C) Facies H. (D) Facies R. (E) Facies G. (F) Facies N

Facies	Subfacies	Component grains	Sedimentary stuctures	Interpretation	Poroperm
M	M - Miliolid facies	Mainly small miliolids	None	Restricted inner ramp (back shoal)	Arith. Mean Ø = 11.0%; Geomean K = 0.97 mD; N = 36
C	CC - *Coskinolina*-dominant facies	*Major:* Large specimens of *Coskinolina* and large rotalids; *Minor:* Small miliolids, rotalids, textulariids and alveolinids	None	Inner ramp (shoal)	Arith. Mean Ø = 13.4%; Geomean K = 1.15 mD; N = 301
	CG - *Coskinolina* grainstone facies	*Major:* Commonly fragmented *Coskinolina*; small and large rotalids, miliolids and textulariids; *Minor:* Alveolinids, rare *Orbitolites* and *Peneroplis*	None	Inner ramp (shoal)	
	CA - *Coskinolina* and *Alveolina* facies	*Major: Coskinolina* and *Alveolina*; *Minor: Orbitolites*, rare undifferentiated soritids and green algae	Rare cross-stratification	Inner ramp (shoal)	
	CP - *Coskinolina* packstone facies	*Major: Coskinolina*	None	Inner ramp (shoal)	
	CH - *Coskinolina* "hash" packstone to wackestone facies	*Major:* Coskinolinid debris	None	Proximal mid-ramp	
H	H - "Hash" facies with fine skeletal debris	*Major:* Finely comminuted bioclasts, rotalid and echinoderm debris	None	Mid-ramp	Arith. Mean Ø = 11.4%; Geomean K = 0.51 mD; N = 92
R	R - Rotalid packstone facies	*Major:* Rotalids (e.g. *Lockhartia*), echinoderm debris	None	Mid-ramp?	Arith. Mean Ø = 16.3%; Geomean K = 2.63 mD; N = 45
	RH - Rotalid "hash" packstone facies	*Major:* Rotalid fragments, finely comminuted undifferentiated bioclasts, echinoderm debris	None	Mid-ramp?	
G	G - *Gypsina* wackestone to packstone facies	*Major: Gypsina*; *Minor:* Nummulitids, nummulitiaclastic debris, *Lepidocyclina*, Operculina	None	Outer ramp	Arith. Mean Ø = 19.7%; Geomean K = 2.89 mD; N = 5
N	N - Nummulitid grainstone to wackestone facies (partially dolomitised)	*Major:* Nummulitids	None	Outer ramp	Arith. Mean Ø = 13.1%; Geomean K = 0.70 mD; N = 18
	AN - Nummulitid wackestone to packstone facies with alveolinids	*Major:* Nummulitids, alveolinids; *Minor:* Operculina	None	Outer ramp	
	ND - Nummulitid facies with discocyclinids (partially dolomitised)	*Major:* Nummulitids, discocyclinids	None	Outer ramp	

Table 1 – Summary of facies for the Bassein Limestone and Panna-Mukta Fields.

Porosity Evolution in the Bassein Limestone of Panna and Mukta Field, Offshore Western India: Burial Corrosion and Microporosity Development

BG GROUP

4. Diagenesis

The Principal diagenetic phases are illustrated in Fig. 6 and 7. The Bassein B units were stabilised and cemented, probably in marine and meteoric-derived fluids. The presence of nodular fabrics suggests that extensive early cementation took place during shallow marine burial. The unconformity and palaeokarst horizon at the top of the B Upper would have led to meteoric cementation. Bassein A limestones and the Alternations have ferroan cements and differ in diagenetic style from the Bassein B. It is likely, based on their sequence stratigraphic context, that the former units were not flushed with shallow meteoric fluids but underwent deeper phreatic stabilisation.

Subsequent burial led to extensive compaction and pressure solution. Stylolites, microstylolites and clay seams developed, enhancing nodular fabrics. At this stage, the Bassein limestones and Alternations would have been tight. Many stylolities developed fractures and tension gashes.

This was followed by mechanical inversion whereby the stylolites where re-opened sufficiently to allow fluids to flow through them and into the host limestones. There followed a major phase of dissolution. This was initially selective, removing the micritic matrix and grains, but corrosion eventually destroyed even calcite spar cements. This was followed by calcite cementation and saddle dolomite. There is some ambiguity over the relative timing of some fractures and saddle dolomite precipitation. In some fractures with apparently un-corroded margins there is a distinct generation of bladed, un-corroded non-ferroan calcite, commonly encased in saddle dolomite that was later etched, locally partly covered with pyrite, followed by dickite precipitation. These could represent fractures that were not affected by the main phase of corrosion but were subject to a later phase of corrosion prior to dickite precipitation. Alternatively, these features could represent a second phase of fracturing after the main corrosion event. Saddle dolomite also occurs in fractures that were already clearly corroded before dolomite precipitation and the dolomite was itself clearly affected by corrosion associated with dickite.

The paragenetic sequence described above (e.g. dickite post-dating major corrosion) is consistent with a mixing corrosion model of porosity development (*cf.* Esteban & Taberner, 2003). Dissolution via acidic fluids generated from CO_2 during thermal maturation of organic matter can be ruled out. The Panna Formation is a Type III source rock and could therefore, on mass balance grounds, generate some CO_2 for the production of leaching fluids. However, this would require a minimum organic carbon content of 5 % assuming that the inorganic component of the source rock has only 30 % of the reactive minerals of the average shale (Giles & Marshall, 1986). This is not the case in the Panna Formation where mean TOC is < 5 %.

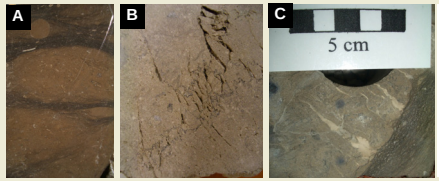

Fig. 6 – (A) Nodular fabric from TZ3 showing burrow fills and clay seams. (B) Stylolite-related fractures and tension gashes. (C) Dickite in fractures related to swarms of microstylolites. (D) Corrosional porosity along stylolite. (E) Corroded saddle dolomite in fracture. (F) Typical corroded matrix with microporosity. (G) Bladed non-ferroan calcite and saddle dolomite (both corroded) and dickite. (H) Fracture-filling saddle dolomite that has been partly replaced by pyrite. (I) Dickite filling a vug in microporous matrix.

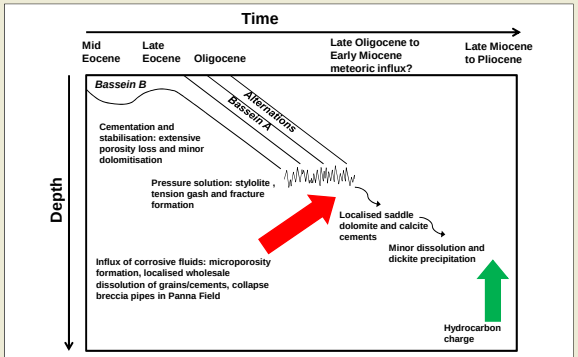

Fig. 7 – Simplified paragenetic sequence for the Panna and Mukta Fields.

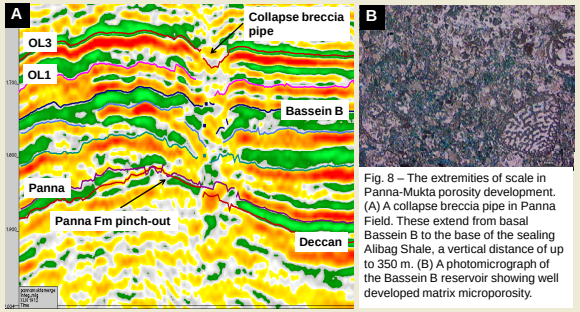

Fig. 8 – The extremities of scale in Panna-Mukta porosity development. (A) A collapse breccia pipe in Panna Field. These extend from basal Bassein B to the base of the sealing Alibag Shale, a vertical distance of up to 350 m. (B) A photomicrograph of the Bassein B reservoir showing well developed matrix microporosity.

Formation/Reservoir	Pore Size	Pore Throat Diameter	Source
Numerous examples	5-10 µm	0.5-2.0 µm	Moshier (1989a)
Thamama Gr., Lower Cretaceous, U.A.E.	Generally 2-4 µm; rarely > 10 µm	Mainly < 2.0 µm	Moshier (1989b)
Haynesville Fm., Upper Jurassic, East Texas	Mainly < 10 µm	Few microns or less	Dravis (1989)
Arab Fm., Upper Jurassic, Saudi Arabia	≤ 10 µm	≤ 1 µm	Cantrell & Hagerty (1999)
Shuaiba Fm., Lower Creatceous, Oman	Mainly 5-10 µm; rarely up to 62 µm	N/A	Al-Awar & Humphrey (2000)
Greenbrier Gr., Lower Carboniferous, U.S.A.	1-5 µm	N/A	Kelleher & Smosna (1993)
Numerous examples	10-60 µm	N/A	Lonoy (2006)
Numerous examples	N/A	< 0.5 µm	Schlumberger
Mishrif Fm., Upper Cretaceous, Iraq; Arab Fm., Upper Jurassic, U.A.E.; Kharaib Fm., Lower Cretaceous, U.A.E.	< 10 µm	N/A	Lambert *et al.* (2006)
Urgonian Limestone Fm., Lower Cretaceous, southern France	N/A	1-2 µm	Richard *et al.* (2007)
Miocene, Madrid Basin, Spain	2-10 µm	N/A	Wright *et al.* (1997)
Arab Fm., Upper Jurassic, Saudi Arabia	≤ 10 µm	≤ 1 µm	Clerke *et al.* (2008); Type 1 microporosity
Numerous examples	N/A	≤ 3 µm	Volery *et al.* (2009)

Table 2 – Documented occurrences and definitions of microporosity based on pore size and pore throat diameter.

5. Pore Systems

Burial corrosion produced a range of porosity types at greatly varying scales. These include matrix microporosity, mouldic macroporosity, vugs, solution-enlarged stylolites and fractures through to the collapse breccia pipes which extend from the top to the base of the reservoir section (Fig. 8). However, while the geologists eyes are naturally drawn to the more spectacular macroporosity, by far the most significant porosity type in terms of total pore volume is matrix and, to a lesser extent, intraparticle microporosity.

6. Microporosity – A Problem of Definition

Microporosity occurs in carbonate reservoirs of all ages and affects their fluid flow properties as well as their log responses. The presence of micropores increases the capillary attraction to the wetting phase (typically water) and frequently results in abundant bound water in the micropores. Consequently, log calculations may then yield high water saturations resulting in erroneous hydrocarbon estimates (Pittman, 1971; Asquith, 1986). Based on log calculations alone, one might not identify a reservoir that would produce little, if any water (Cantrell & Hagerty, 1999), a characteristic termed “Low Resistivity Pay” (LRP). Additional considerations are the poroperm relationships and the resulting fluid flow properties inherent to micropore-dominated carbonate reservoirs, notably very high porosities but low permeabilities. However, despite the volumetric significance of microporosity in many carbonate reservoirs and the associated reservoir characterisation challenges, microporosity in carbonate rocks remains both poorly defined and poorly understood.

The principal stumbling block when trying to meaningfully discuss microporosity is the many, varying definitions that exist in the literature. This is exacerbated by the fact that geologists, petrophysicists and engineers often have their own definitions. Furthermore, the precise definition often depends on the method of observation. For example, the geologist looking at thin-sections will typically define microporosity differently to the petrophysicist working with T_2 cut-offs from NMR logs.

If we consider pore size as observed with a standard petrographic or scanning electron microscope (SEM), it can be seen that most authors place the upper limit for microporosity at 10 µm. In terms of pore throat diameter determined by mercury porosimetry, there appears to be a convergence in the literature at *ca.* 2 µm (Table 2). Consequently, an upper size limit of ≤ 2 µm appears to be most appropriate. This is consistent with the synthesis of Zinszner & Pellerin (2007) which demonstrates that even ‘pure’ micrites lacking visible porosity in thin-section are dominated by pore throat diameters of 1 µm or slightly larger. It is also supported by the porosimetry work of Richard *et al.* (2007) who show that micrite matrix and peloids in ‘chalky’ Cretaceous limestones in southeastern France have pore throats of 1.04 to 2.13 µm. This differs from the definition favoured by Schlumberger (*cf.* Ahr *et al.* 2005) who define micropores as those pores with pore throat diameters ≤ 0.5 µm and usually contain mostly irreducible water and little hydrocarbon. By this definition most of the published geological descriptions of microporosity would actually be mesoporosity (Table 2 & Fig. 9). Clerke *et al.* (2008) propose an alternative scheme recognising three types of microporosity based on pore throat size (Fig. 9). This classification is useful in that it recognises that a spectrum of microporosity exists based on pore throat diameter from that which is effectively tight (types 2 and 3) to that which can store and flow hydrocarbons (type 1; Fig. 9).

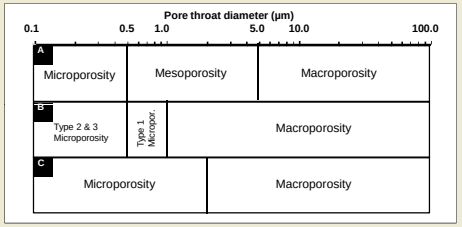

Fig. 9 – Different porosity classifications and microporosity definitions based on pore throat diameter. (A) Schlumberger scheme (B) Clarke *et al.* (2008) scheme based on Arab Fm in Saudi Arabia (C) Proposed scheme based on published geological descriptions of microporosity (*cf.* Table 2).

Andrew J. Barnett, V. Paul Wright & Mohit Khanna

New Orleans 2010

Porosity Evolution in the Bassein Limestone of Panna and Mukta Field, Offshore Western India: Burial Corrosion and Microporosity Development

BG GROUP

6. Microporosity – A Problem of Definition (cont.)

In terms of occurrence, two major types of microporosity can be recognised: (1) matrix microporosity and (2) intraparticle microporosity. In both (1) and (2), the porosity is hosted in a mosaic of micron to sub-micron-scale calcite crystals. In some microporous carbonate reservoirs this takes the form of pristine micro-rhombic calcite crystals; in others in which the microporosity has been created or enhanced by dissolution, individual crystals may have a ragged irregular appearance. In some carbonate reservoirs, these pore types can make up the bulk of, if not all of the pore volume.

Microporosity in carbonate rocks is sometimes referred to as 'chalky' porosity and samples exhibiting microporosity as 'chalky textured'. A distinction must be made between microporous limestones and true chalks. Chalks are fine-grained carbonate rocks predominantly composed of pelagic nanno- and microfossils deposited on deeper shelves and in basins (Flugel, 2004). In chalks, porosity occurs as intraparticle and interparticle porosity hosted within and between these fossils respectively. As will be seen later, this is not purely an academic distinction but has significant implications in terms of pore throat size and poroperm characteristics.

7. A Spectrum of Microporosity Development: Pore Throat Size and Poroperm Characteristics

Fig. 10 is a poroperm cross-plot for two North Sea chalks (Tor and Ekofisk Formations), microporous limestone from several Shuaiba Formation reservoirs in the Middle East and Bassein B reservoir from BG's Mukta Field, offshore India. Fig. 11 shows mercury injection capillary pressure (MICP) derived pore throat diameters from a representative subset of the same data. Accompanying photomicrographs show porosity development and associated variations in pore throat size (Fig. 12).

Note that both of the North Sea chalks plot on lower poroperm trends than the microporous limestones of the Shuaiba Formation (Fig. 10). This is because, although the North Sea chalk and Shuaiba reservoirs are both dominated by microporosity, pore throat sizes are smaller in chalk than in other microporous limestones (Fig. 11). The difference between the Tor and Ekofisk Formation can be explained in the same way. Both of these chalks effectively plot on grain-size trends, the Ekofisk being finer than the Tor. Consequently, the Ekofisk Formation chalk has smaller pore throats and lower permeability than that of the Tor Formation.

Important variations in poroperm occur within the Shuaiba Formation dataset. These can also be explained in terms of pore throat size. As already noted, microporosity occurs in the intercrystalline voids within micro-rhombic calcite mosaics. The resulting pore system has homogeneous pore throat size distributions due to the relatively uniform size of the calcite crystals. However, in some cases, these micro-rhombic crystal mosaics have undergone a later phase of dissolution which reduces crystal size giving a corresponding increase in pore throat size and permeability. This is clearly visible in Fig. 12 which shows a higher permeability sample in which individual crystals are rounded due to corrosion. Similar observations have been made for Jurassic and Cretaceous carbonate reservoirs in the Middle East (Lambert *et al.*, 2006).

The Bassein B reservoir of Mukta Field is not a classic microporous reservoir like the Shuaiba Formation, but is rather a bimodal porosity reservoir which has some macroporosity in addition to abundant microporosity (Table 3). This is clearly reflected in the poroperm trend and pore throat size distributions for this reservoir. The vast majority of the preserved porosity in Mukta Field is due to late burial dissolution. Consequently, Mukta is another example of a leached microporous mosaic. However, in this case, dissolution has gone a step further than that seen in the Shuaiba Formation datasets and has produced not only a solution-enhanced micropore system but also a macropore network. Note that despite the presence of up to 40 % macroporosity, the abundance of microporosity still plays a key role in determining permeability (Fig. 13).

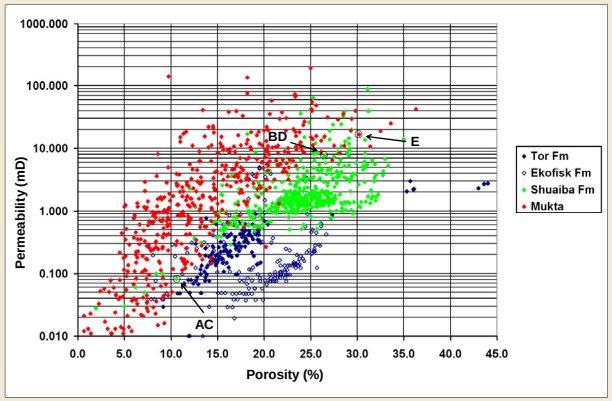

Fig. 10 – Poroperm cross-plot for two North Sea chalk reservoirs (Tor and Ekofisk Formations), the Shuaiba Formation (data is from several Shuaiba reservoirs in Oman and the U.A.E.) and the Bassein B reservoir of Mukta Field, offshore India. The separation of these datasets into relatively discrete fields is due to variations in pore throat size (see Fig. 11). The letters refer to the photomicrographs in Fig. 12.

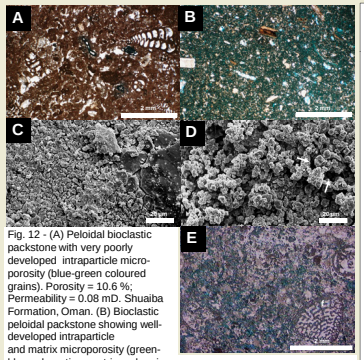

Fig. 12 - (A) Peloidal bioclastic packstone with very poorly developed intraparticle micro-porosity (blue-green coloured grains). Porosity = 10.6 %; Permeability = 0.09 mD. Shuaiba Formation, Oman. (B) Bioclastic peloidal packstone showing well-developed intraparticle and matrix microporosity (green-blue colouration; matrix and grains are difficult to distinguish due to pervasive nature of microporosity development). Porosity = 26.5 %; Permeability = 7.85 mD. Shuaiba Formation, Oman. (C) SEM photomicrograph showing the micropore network of the sample shown in (A). Although individual crystals appear to have undergone dissolution (note their irregular shape), subsequent compaction and/or cementation has narrowed pore throats resulting in an ineffective pore system with negligible permeability. (D) SEM photomicrograph showing the micropore system of the sample in (B). Although some crystals retain a micro-rhombic morphology, the vast majority are strongly corroded. Note the irregular pores (microvugs; examples are arrowed) which are often several times larger than individual crystals. (E) Bioclastic packstone with very well-developed matrix and intraparticle (in foraminifera – f) microporosity. Porosity = 30.2 %; Permeability = 16.7 mD. Bassein Formation, Mukta Field, India.

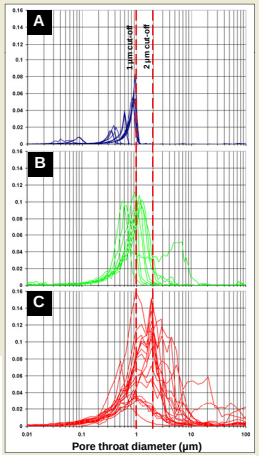

Figure 11 - Mercury porosimetry plots for (A) North Sea chalk (Tor and Ekofisk Formations), (B) Shuaiba Formation and (C) Bassein B reservoir (Mukta Field, offshore India). Microporosity, here defined as pores with pore throat diameters of ≤ 2 µm (the 1 µm cut-off favoured by some workers is also shown), comprises a very significant proportion of the pore volume of both the Shuaiba and Bassein B reservoirs (see Table 3).

Reservoir	N	Min Microporosity (%)	Max Microporosity (%)	Mean Microporosity (%)
Shuaiba Fm *(1 µm cut-off)*	10	34.3	91.4	65.5
Shuaiba Fm *(2 µm cut-off)*	10	52.0	98.0	90.1
Bassein B *(1 µm cut-off)*	22	26.0	90.6	47.1
Bassein B *(2 µm cut-off)*	22	41.3	94.4	69.9

Table 3 – Microporosity abundance as a proportion of total porosity based on MICP data. Results using both 1 µm and 2 µm cut-offs are shown as a sensitivity test of the varying definitions favoured by different workers.

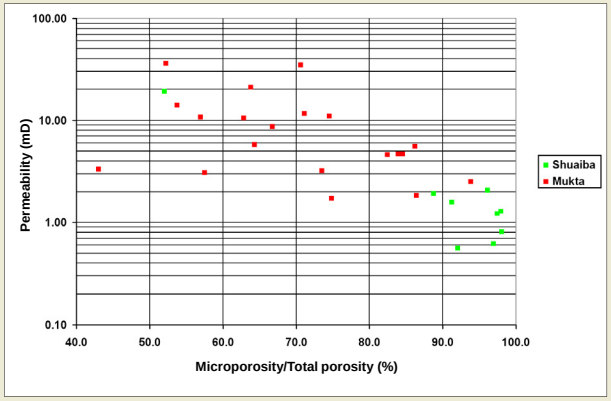

Fig. 13 - Cross-plot of microporosity as a proportion of total porosity versus permeability.

8. Conclusions

- The Bassein Formation Eocene-Oligocene ramp carbonates of Panna and Mukta Fields are examples of limestones which underwent extensive to complete porosity loss in shallow burial environments prior to a major phase(s) of burial corrosion producing all current porosity.

- The diagenetic characteristics and paragenetic sequence exhibited by these limestones is consistent with a mixing corrosion model of porosity development. Major dissolution by acidic fluids generated from CO_2 or carboxylic acids can be ruled out because mass balance calculations show that the TOC of the Panna Formation source rocks is not sufficient for these other late dissolution mechanisms to be significant.

- Burial corrosion produced porosity at a variety of scales from matrix microporosity to mm-scale vugs and solution-enlarged stylolites to collapse breccia pipes up to 350 m in length which vertically cross-cut the entire reservoir section. However, matrix and intraparticle microporosity are by far the most signficant in terms of total pore volume.

- Considerable confusion has been caused by the use of different definitions of microporosity in the literature and this frequently hampers communication between geologists, petrophysicists and reservoir engineers. The plethora of definitions currently in use is due to the varied techniques used to detect and quantify microporosity (e.g. T_2 cut-offs from NMR logs, MICP-derived pore throat diameters, pore size from thin-section observation).

- A comparison with chalk (*sensu stricto*) reservoirs and other microporous limestones suggests that a spectrum of microporosity occurs characterised by increasing pore size from (1) chalk reservoirs with intra- and interparticle porosity hosted in and/or between pelagic nanno- and microfossils, (2) matrix and intraparticle microporosity occurring in relatively pristine (i.e. mainly non-leached) micro-rhombic calcite mosaics (e.g. many Cretaceous limestone reservoirs in the Middle East) and (3) corrosion-enhanced matrix and intraparticle microporosity in which calcite crystals have been rounded and reduced in size thereby increasing pore throat diameter (e.g. some Cretaceous reservoirs in the Middle East, Bassein B reservoir of the Panna and Mukta Fields).

Andrew J. Barnett, V. Paul Wright & Mohit Khanna

New Orleans 2010